Supporting Information

Structural Insights into Ni-stabilized Fe-rich High Voltage Spinels: $LiNi_xFe_{0.5-x}Mn_{1.5}O_4$

Anna Windmüller[*], *Tingting Yang, Kristian Schaps, Anna Domgans, Frederik Zantis, Baolin Wu, Leyela Hassen Adem, Bikila Nagasa Olana, Chih-Long Tsai, Shicheng Yu, Luc Raijmakers, Hans Kungl, Hermann Tempel, Rafal E. Dunin-Borkowski, Shawn D. Lin, Mirijam Zobel, Bing Joe Hwang, Rüdiger–A. Eichel*

A. Windmüller, K. Schaps, A. Domgans, F. Zantis, B. Wu, C.-L. Tsai, S. Yu, L. Raijmakers, H. Kungl, H. Tempel, R.-A. Eichel
Institute for Energy Technologies (IET–1: Fundamental Electrochemistry), Forschungszentrum Jülich, D–52425 Jülich, Germany
a.windmueller@fz-juelich.de

T. Yang, R. E. Dunin-Borkowski
Ernst Ruska-Centre for Microscopy and Spectroscopy with Electrons (ER-C-1), Forschungszentrum Jülich, 52425 Jülich, Germany

A. Domgans, F. Zantis, B. Wu, R.-A. Eichel
RWTH Aachen University, Institute of Physical Chemistry, D-52074 Aachen, Germany

L. H. Adem, B. N. Olana, S. D. Lin
Department of Chemical Engineering, National Taiwan University of Science and Technology, Taipei 10617, Taiwan

M. Zobel
Institute of Crystallography, RWTH Aachen University, 52066 Aachen, Germany

M. Zobel
Jülich Centre for Neutron Science - Neutron Analytics for Energy Research (JCNS-3), Forschungszentrum Jülich GmbH, Wilhelm-Johnen-Straße, 52428 Jülich, Germany

B. J. Hwang
Department of Chemical Engineering, Nano-electrochemistry Laboratory, National Taiwan University of Science and Technology, 106 Taipei City, Taiwan.

B. J. Hwang
Sustainable Electrochemical Energy Development Center, National Taiwan University of Science and Technology, 106 Taipei City, Taiwan

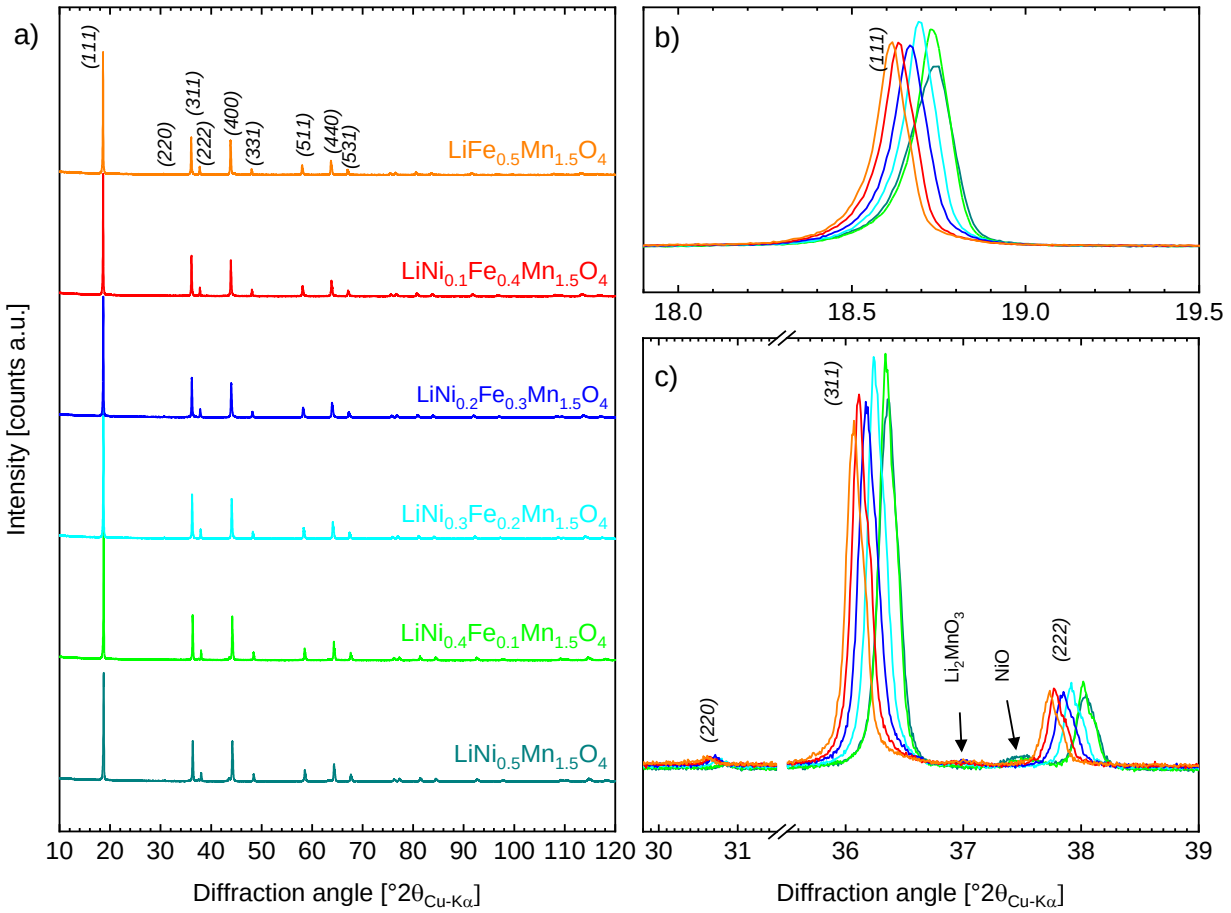

Figure S1: XRD results of $LiNi_xFe_{0.5-x}Mn_{1.5}O_4$: a) all samples diffractograms from 10 to 120 °2θ, the diffraction patterns are stacked vertically with offsets, indexation based on Fd-3m. b) Magnification from 18 to 19.5 °2θ, showing the main 111 reflection for all samples. c) Magnification from 30 to 39 °2θ, showing the spinel 220, 311 and 222 reflection and reflections from the Li_2MnO_3 and NiO secondary phases.

Table S1: Calculated mole per formula unit $LiNi_xFe_{0.5-x}Mn_{1.5}O_4$ of ICP-OES elemental analysis

Element	x in $LiNi_xFe_{0.5-x}Mn_{1.5}O_4$					
	0.5	0.4	0.3	0.2	0.1	0
Li	0.99	0.98	0.99	0.98	0.99	0.98
Ni	0.49	0.40	0.28	0.19	0.10	0.00
Fe	0.00	0.10	0.20	0.29	0.39	0.49
Mn	1.52	1.51	1.54	1.53	1.52	1.53

a)

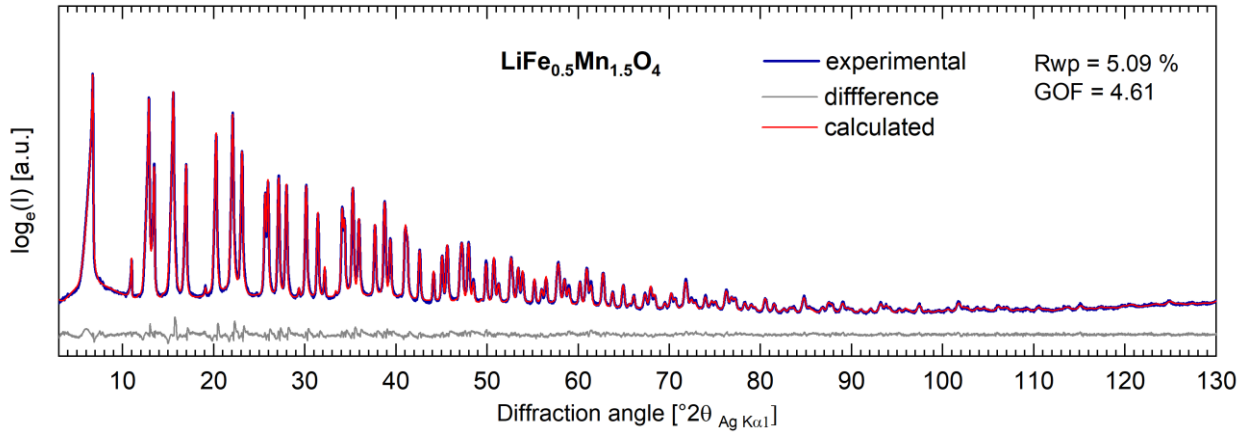
LiFe0.5Mn1.5O4
experimental
diffference
calculated
Rwp = 5.09 %
GOF = 4.61
loge(I) [a.u.]
10 20 30 40 50 60 70 80 90 100 110 120 130
Diffraction angle [°2θ Ag Kα1]

b)

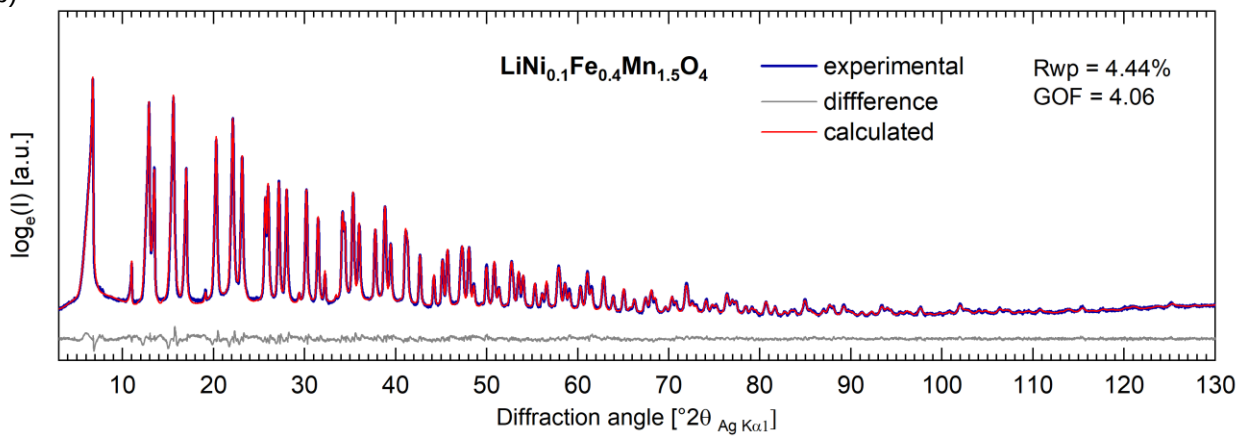
LiNi0.1Fe0.4Mn1.5O4
experimental
diffference
calculated
Rwp = 4.44%
GOF = 4.06
loge(I) [a.u.]
10 20 30 40 50 60 70 80 90 100 110 120 130
Diffraction angle [°2θ Ag Kα1]

c)

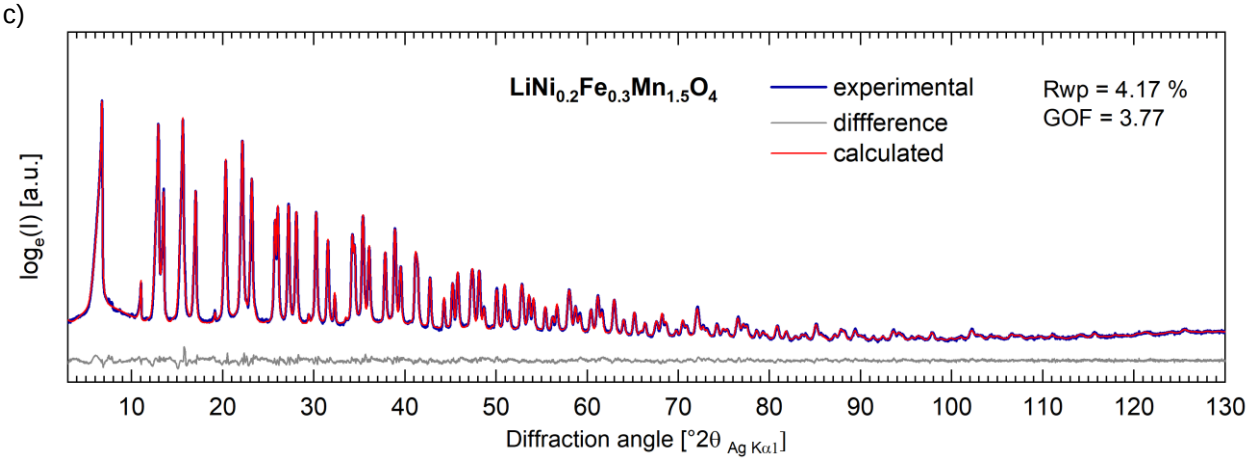
LiNi0.2Fe0.3Mn1.5O4
experimental
diffference
calculated
Rwp = 4.17 %
GOF = 3.77
loge(I) [a.u.]
10 20 30 40 50 60 70 80 90 100 110 120 130
Diffraction angle [°2θ Ag Kα1]

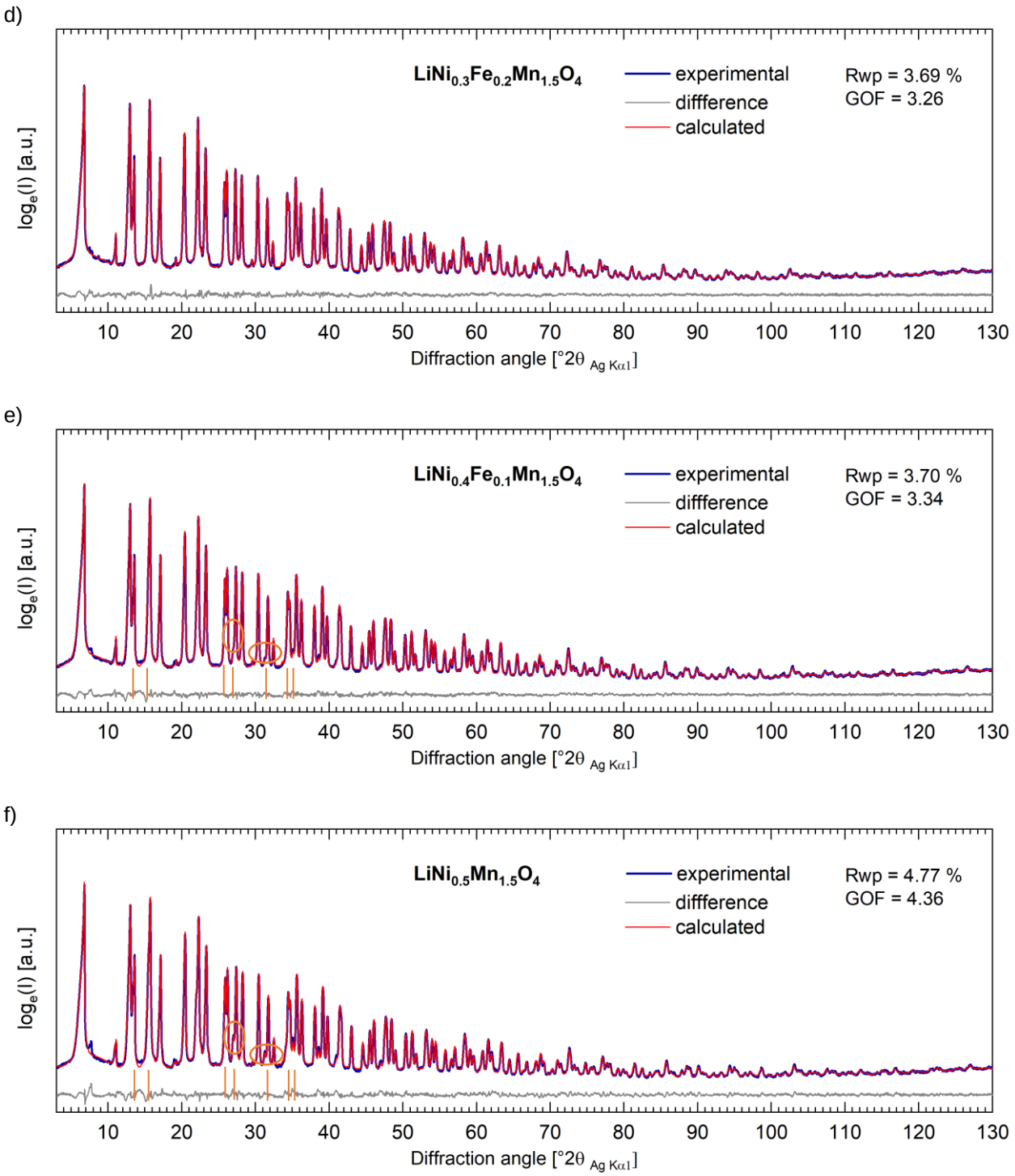

Figure S2: Fitting results from Rietveld analysis based on Ag $K\alpha_1$ PXRD data for $LiNi_xFe_{0.5-x}Mn_{1.5}O_4$: a) x = 0, b) x = 0.1, c) xv= 0.2, d) x= 0.3, e) x = 0.4, f) x = 0.5 – Orange lines mark positions of NiO reflections. Circles guide the eye to freestanding NiO reflections.

Table S2: Results from Rietveld analysis based on Ag $K\alpha_1$ PXRD data for $LiNi_xFe_{0.5-x}Mn_{1.5}O_4$ (x = 0, 0.1, 0.2, 0.3, 0.4, 0.5), in spinel structure Fm-3m. Wyckoff position 8a: 1/8, 1/8, 1/8; and 16d: 1/2, 1/2, 1/2,. Secondary phase as NiO in Fm-3m for x = 0.4 and x = 0.5.

x	Lattice parameters [Å]	NiO wt.-%	Fe occupancy at 8a site	x=y=z fractional coordinate 32e site	Bond distance 8a-32e	Bond distance 16d-32e
0.0	8.2473(3)		0.0224(11)	0.26345(5)	1.9774(8)	1.9574(4)
0.1	8.2369(4)		0.0270(10)	0.26325(5)	1.9717(7)	1.9554(3)
0.2	8.2266(2)		0.0314(9)	0.26322(4)	1.9694(6)	1.9540(3)
0.3	8.2045(2)		0.0278(8)	0.26314(4)	1.9631(5)	1.9493(3)
0.4	8.1837(2)	1.5	0.0089(8)	0.26323(4)	1.9595(6)	1.9440(3)
0.5	8.1785(3)	4.0	0	0.26317(5)	1.9573(7)	1.9429(4)

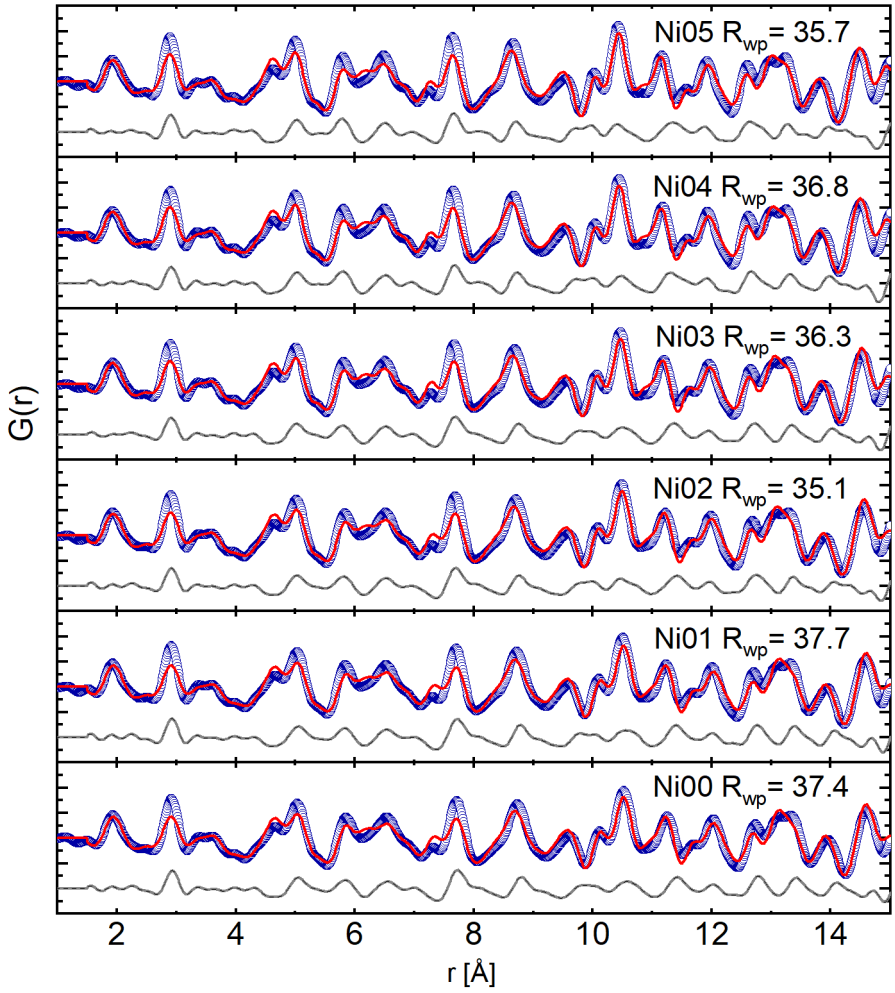

Figure S3: Fitting results from PDF analysis based on Ag $K\alpha_1$ PXRD data for $LiNi_xFe_{0.5-x}Mn_{1.5}O_4$: Ni00: x = 0; Ni01: x = 0.1; Ni02 x = 0.2; Ni03: x = 0.3; Ni04: x = 0.4; Ni05: x = 0.5. Fit model: average structure only. Blue circles: experimental, red lines: calculated, gray: difference.

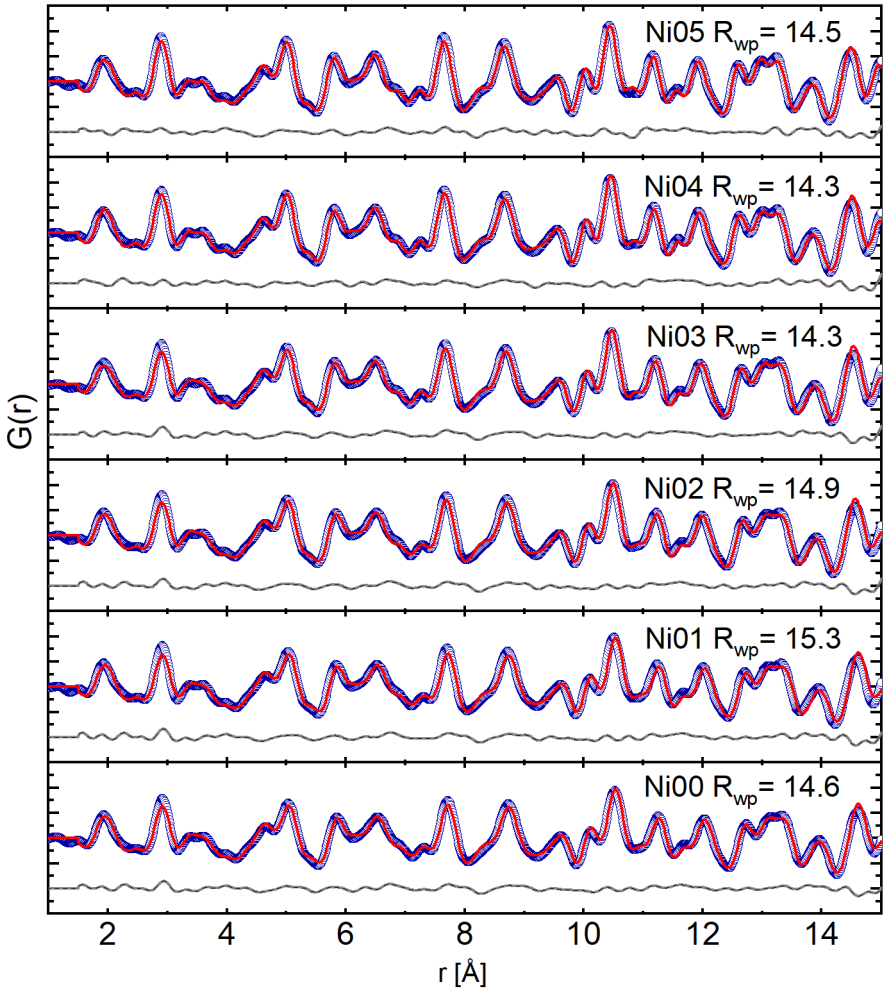

Figure S4: Fitting results from PDF analysis based on Ag $K\alpha_1$ PXRD data for $LiNi_xFe_{0.5-x}Mn_{1.5}O_4$: Ni00: x = 0; Ni01: x = 0.1; Ni02 x = 0.2; Ni03: x = 0.3; Ni04: x = 0.4; Ni05: x = 0.5. Fit model: average structure + B_{iso} + Fe occupancies at 8a. Blue circles: experimental, red lines: calculated, gray: difference.

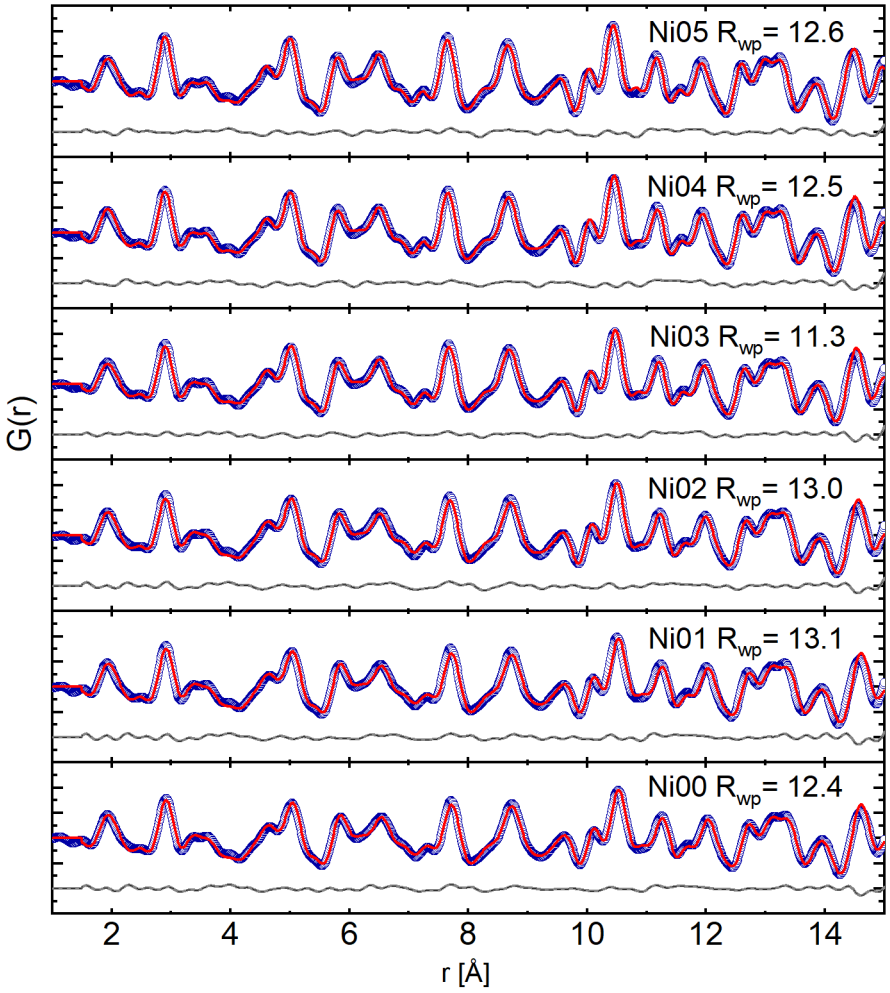

Figure S5: Fitting results from PDF analysis based on Ag Kα$_1$ PXRD data for $LiNi_xFe_{0.5-x}Mn_{1.5}O_4$: Ni00: x = 0; Ni01: x = 0.1; Ni02 x = 0.2; Ni03: x = 0.3; Ni04: x = 0.4; Ni05: x = 0.5. Fit model: full model including Li_2MnO_3 fractions under spherical damping. Blue circles: experimental, red lines: calculated, gray: difference.

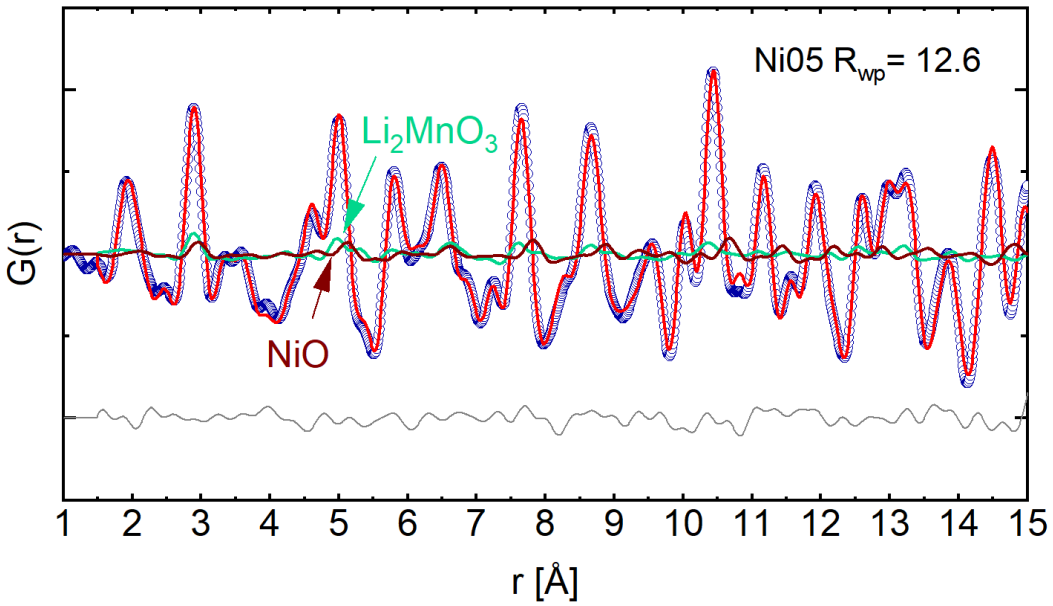

Figure S6: Detailed view of fitting results from PDF analysis based on Ag $K\alpha_1$ PXRD data for $LiNi_{0.5}Mn_{1.5}O_4$. Fit model: full model including Li_2MnO_3 fractions under spherical damping and NiO. Blue circles: experimental, red lines: calculated, gray: difference.

Table S3: Results from PDF analysis based on Ag $K\alpha_1$ PXRD data for $LiNi_xFe_{0.5-x}Mn_{1.5}O_4$ (x = 0, 0.1, 0.2, 0.3, 0.4, 0.5), in spinel structure Fm-3m. 8a: 1/8, 1/8, 1/8; 16d: 1/2, 1/2, ½. Secondary phase as NiO in Fm-3m for x = 0.4 and x = 0.5. The secondary phase Li_2MnO_3 was refined with space group C2/m with finite size modelled by spherical damping.[1]

x	Lattice parameter [Å]	NiO wt.-%	Li_2MnO_3 wt.-%	Li_2MnO_3 finite size [Å]	Fe occupancy at 8a site	Isotropic displacement parameter O at 32e [nm²]	Isotropic displacement parameter TM at 16d [nm²]
0.0	8.2551(5)		20.2	13(1)	0.489(6)	2.23(4)	0.55(1)
0.1	8.2414(5)		13.6	15(1)	0.545(6)	2.33(4)	0.52(1)
0.2	8.2264(5)		10.8	29(1)	0.629(6)	1.97(3)	0.52(1)
0.3	8.2092(6)		11.9	40(1)	0.427(6)	1.81(3)	0.45(1)
0.4	8.1924(6)	1.5	14.0	39(1)	0.028(7)	2.02(3)	0.43(1)
0.5	8.1833(5)	4.3	14.4	31(1)	0	2.50(3)	0.44(1)

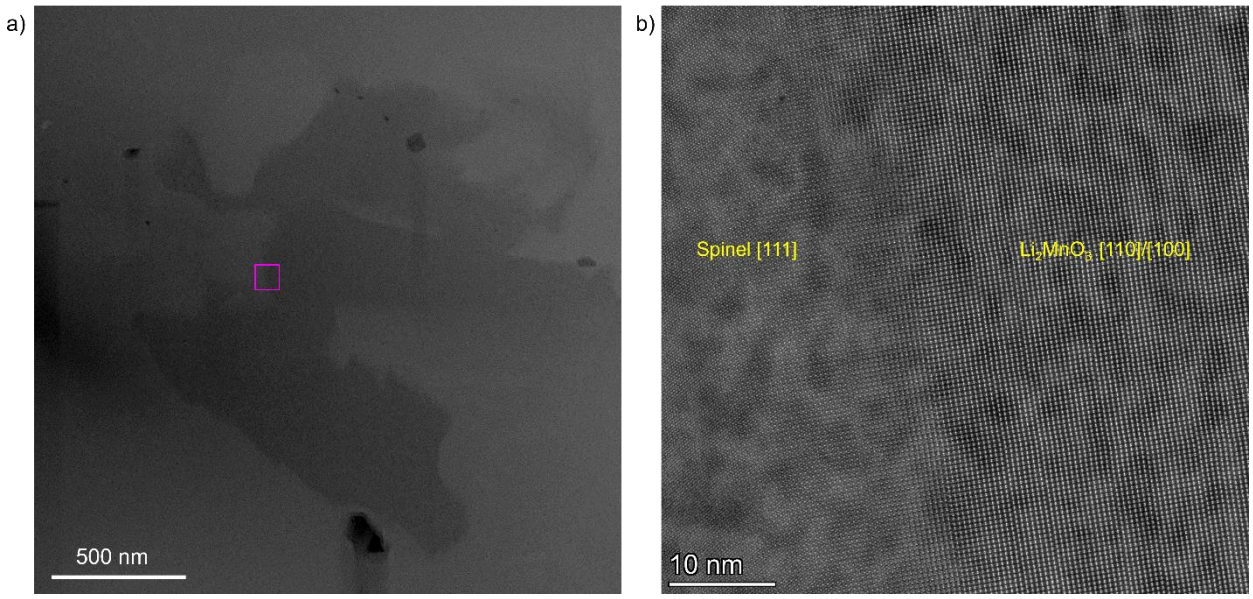

Figure S7. The atomic HAADF-STEM image of the $LiNi_{0.2}Fe_{0.3}Mn_{1.5}O_4$, which exhibited two different phases in the selected region.

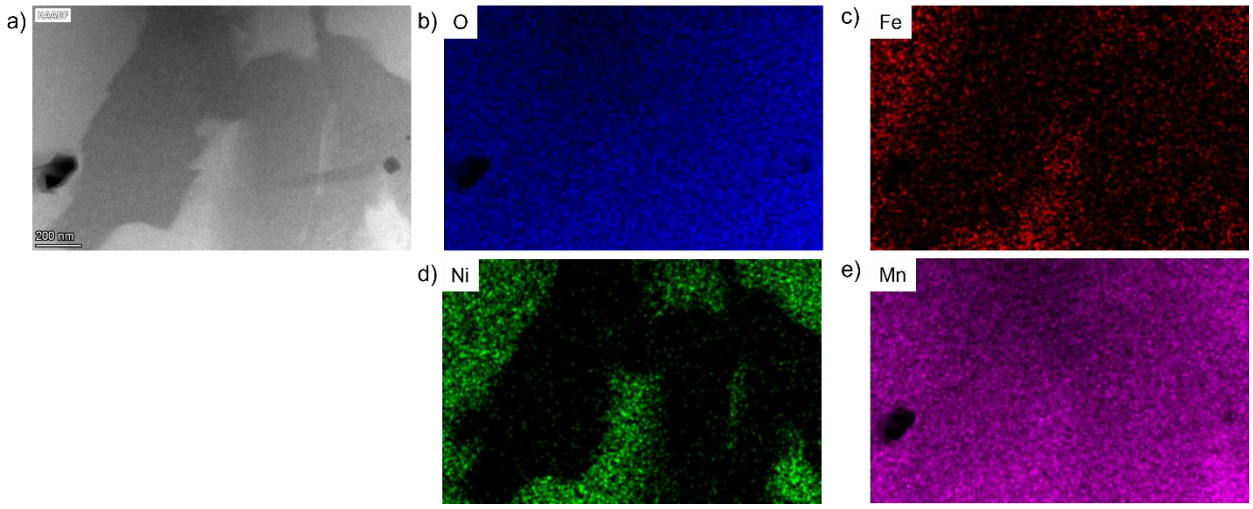

Figure S8. a) HAADF image of the $LiNi_{0.2}Fe_{0.3}Mn_{1.5}O_4$ sample and the corresponding EDS mappings including b) oxygen, c) iron, d) nickel, and e) manganese, which exhibit non-uniform distributions of the elements.

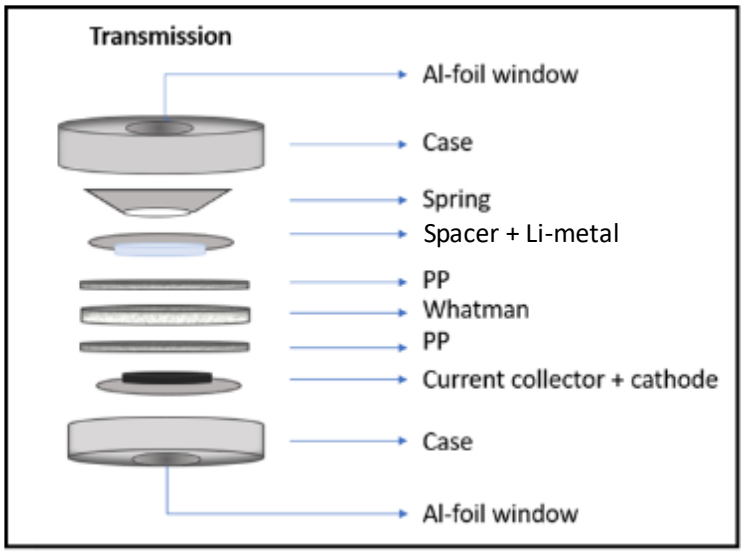

Figure S9: Cell design of in-situ cell for transmission geometry. Al foil is used as window (2x) and as current collector (1x) giving rise to 3 different Al signals in the diffraction pattern due to different displacements towards the beam.

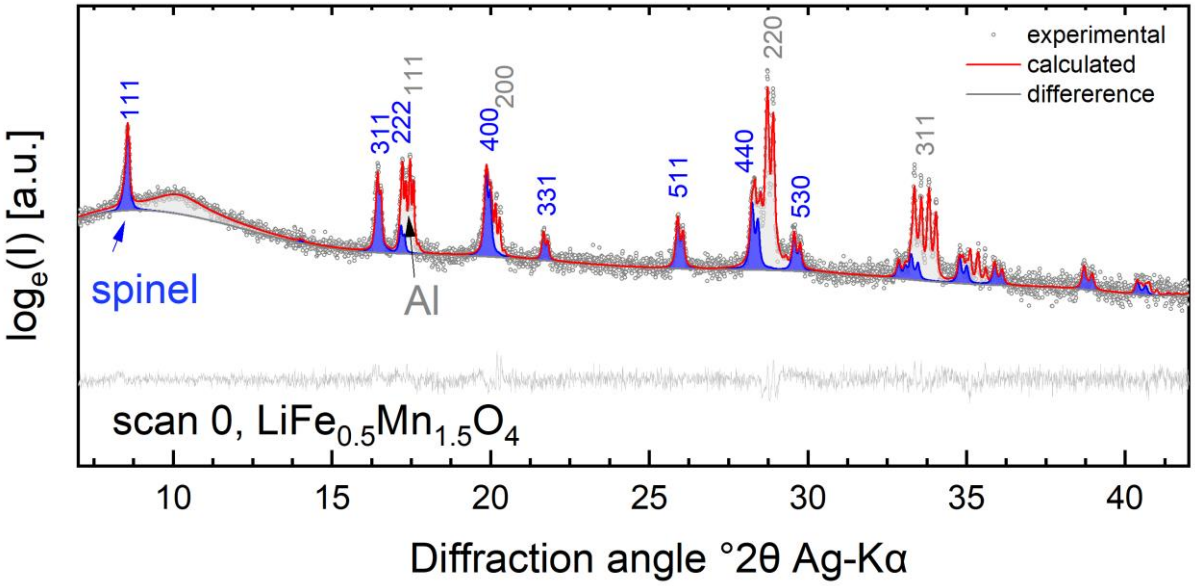

Figure S10: Example fit for from the in-situ PXRD analysis: $LiFe_{0.5}Mn_{1.5}O_4$ scan 0, at the beginning of the in-situ measurment.

Table S3. In situ DRIFTS spectra (cm^{-1}) of LP30 over $LiFe_{0.5}Mn_{1.5}O_4$, $LiNi_{0.1}Fe_{0.4}Mn_{1.5}O_4$ and $LiNi_{0.3}Fe_{0.2}Mn_{1.5}O_4$ at the OCV.

$LiFe_{0.4}Mn_{1.5}O_4$	$LiNi_{0.1}Fe_{0.4}Mn_{1.5}O_4$ and $LiNi_{0.3}Fe_{0.2}Mn_{1.5}O_4$	Reference	Assignment
2966		2989[2], 1997[3], 2906[4]	ν C-H
1782,1763	1720,1819	1763[5], 1762[6],1767[2], 1770[2],	ν C=O of (EC, DMC)
1460, 1356, 1184,	1561,1475	1450[3], 1367[2], 1403[3]	δ C-H
1300, 1250	1324,1276,1159,	1263[5], 1332[6], 1270[4], 1261[3]	νC-O/νs C-O-C
1106, 1057	1073, 960	1086[7], 1070[4]	ν C-O + ν ring, EC
992		1035[7], 1001[4], 944[7]	νC-C
924			ν CH_3-O
829	847	842[2],845[7]	ν P-F, δ -co_3
760		781[4,7], 713[4], 733[3]	δ EC, ring deformation
ν stretch, δ bending			

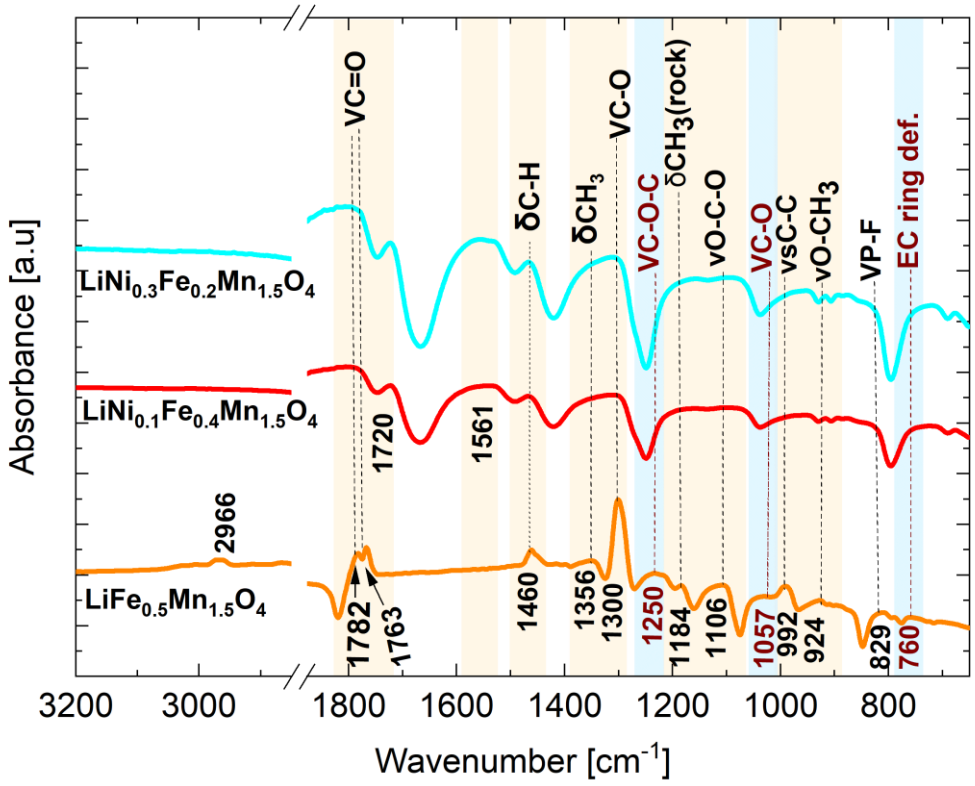

Figure S11: In situ DRIFTS spectra of LP30 over $LiFe_{0.5}Mn_{1.5}O_4$, $LiNi_{0.1}Fe_{0.4}Mn_{1.5}O_4$ and $LiNi_{0.3}Fe_{0.2}Mn_{1.5}O_4$ at the OCV

$LiFe_{0.5}Mn_{1.5}O_4$

1st cycle

2nd cycle

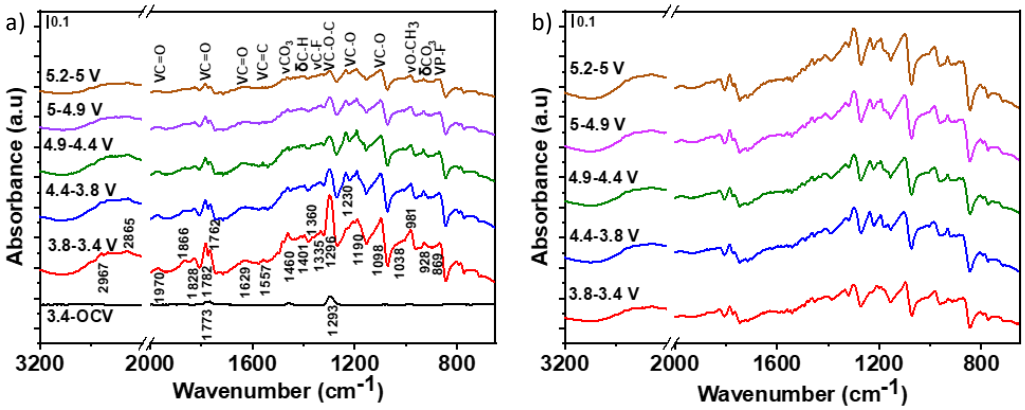

$LiNi_{0.1}Fe_{0.4}Mn_{1.5}O_4$

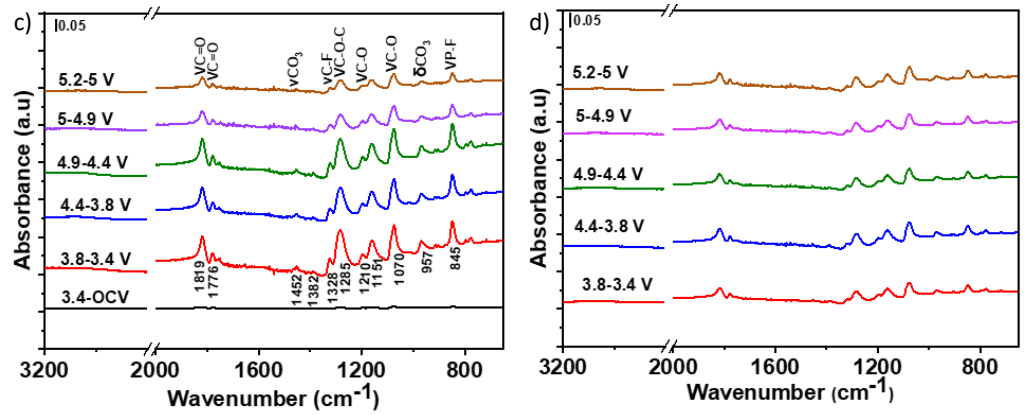

$LiNi_{0.3}Fe_{0.2}Mn_{1.5}O_4$

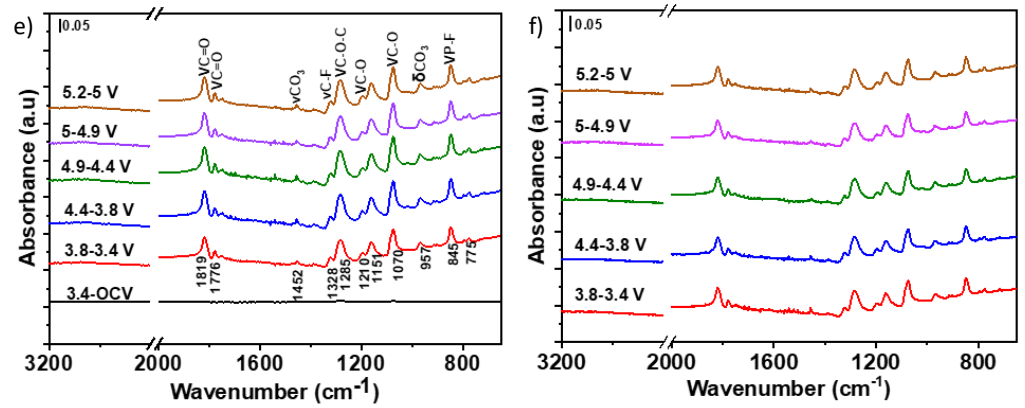

Figure S12: In situ DRIFTS difference spectra of LP30 during delithiation cycle over $LiFe_{0.5}Mn_{1.5}O_4$ 1st (a) and 2nd cycle (b), over $LiNi_{0.1}Fe_{0.4}Mn_{1.5}O_4$ 1st (c) and 2nd cycle (d), and over $LiNi_{0.3}Fe_{0.2}Mn_{1.5}O_4$ 1st (e) and 3rd cycle (f).

[1] T. Egami, S. Billinge, *Materials Today* **2003**, *6*, 57.

[2] Y. B. Yohannes, S. D. Lin, N.-L. Wu, *Journal of The Electrochemical Society* **2017**, *164*, A3641.

[3] Y. B. Yohannes, S. D. Lin, N.-L. Wu, B.-J. Hwang, *Journal of The Electrochemical Society* **2019**, *166*, A2741.

[4] A. M. Haregewoin, E. G. Leggesse, J.-C. Jiang, F.-M. Wang, B.-J. Hwang, S. D. Lin, *13th International Meeting on Lithium Batteries* **2013**, *244*, 318.

[5] B. N. Olana, S. D. Lin, B.-J. Hwang, *Electrochimica Acta* **2022**, *416*, 140266.

[6] Y. Ikezawa, H. Nishi, *Electrochimica Acta* **2008**, *53*, 3663.

[7] A. M. Haregewoin, E. G. Leggesse, J.-C. Jiang, F.-M. Wang, B.-J. Hwang, S. D. Lin, *Electrochimica Acta* **2014**, *136*, 274.